Hindawi Publishing Corporation
EURASIP Journal on Advances in Signal Processing
Volume 2010, Article ID 960831, 9 pages
doi:10.1155/2010/960831

Research Article

Classification of Polarimetric SAR Image Based on Support Vector Machine Using Multiple-Component Scattering Model and Texture Features

Lamei Zhang, Bin Zou, Junping Zhang, and Ye Zhang

Department of Information Engineering, Harbin Institute of Techonology, Harbin, Heilongjiang 150001, China

Correspondence should be addressed to Lamei Zhang, zzbei@hit.edu.cn

Received 25 May 2009; Revised 4 September 2009; Accepted 7 October 2009

Academic Editor: Carlos Lopez-Martinez

The classification of polarimetric SAR image based on Multiple-Component Scattering Model (MCSM) and Support Vector Machine (SVM) is presented in this paper. MCSM is a potential decomposition method for a general condition. SVM is a popular tool for machine learning tasks involving classification, recognition, or detection. The scattering powers of single-bounce, double-bounce, volume, helix, and wire scattering components are extracted from fully polarimetric SAR images. Combining with the scattering powers of MCSM and the selected texture features from Gray-level cooccurrence matrix (GCM), SVM is used for the classification of polarimetric SAR image. We generate a validity test for the proposed method using Danish EMISAR L-band fully polarimetric data of Foulum Area (DK), Denmark. The preliminary result indicates that this method can classify most of the areas correctly.

1. Introduction

Polarimetric SAR (PolSAR) image classification is arguably one of the most important applications in remote sensing. Many supervised and unsupervised classification methods have been proposed. Earlier polarimetric classification methods were based on the supervised method of the statistical characteristics of PolSAR images. Then Cloude and Pottier presented an unsupervised method based on the entropy H and α angle distribution [1]. In 1998, Freeman and Durden suggested a three-component decomposition method of polarimetric data [2], which introduced a combination of surface, double-bounce, and volume scatterings. A combined use of physical scattering characteristics and statistical properties for terrain classification is desirable. L. Ferro- Famil et al. developed some classification methods combining both the target decomposition and complex Wishart classifier [3, 4].

The importance of SAR polarimetry in classification arises principally because polarization is sensitive to orientation. Polarimetric target decomposition theorem expresses the average mechanism as the sum of independent elements in order to associate a physical mechanism with each resolution cell, which allows the identification and separation of scattering mechanisms in polarization signature for purposes of classification and recognition. Several decomposed methods have been proposed to identify the scattering characteristics based on polarimetric statistical characteristics [1, 2, 5–7]. Multiple-Component Scattering Model (MCSM) is a general polarimetric target decomposition method, which can be applied to the symmetry and asymmetry reflection conditions [8].

Some classification methods, such as statistic classifiers and Neural Network (NN) classifier [9], have been used in the classification. However, the former needs the statistic information of the training samples, and the later usually converges slowly and tends to converge to a local optimization.

Support Vector Machine (SVM) has become an increasing popular tool for machine learning tasks involving classification, recognition, or detection. SVM is based on statistic learning theorem; however, SVM method does not

need the statistic features of the training samples and it can deal with high dimension data and nonlinear problem easily and can also achieve global optimization [10–14].

In this paper, we propose a classification method which combines MCSM and SVM. The brief descriptions of MCSM and GCM are given in Sections 2 and 3, respectively. In Section 4, the theorem of SVM is summarized. Based on these theoretical analyses, the L-band EMISAR polarimetric SAR data has been used to demonstrate application of MCSM and SVM to classification in Section 5. Finally, the conclusion and discussions are presented in Section 6.

2. Multiple-Component Scattering Model

2.1. Scattering Vector and Covariance Matrix. The fully polarimetric SAR measures the amplitude and phase of backscattering signals in the four combinations of the linear receive and transmit polarizations: HH, HV, VH, and VV. These signals form a complex scattering matrix $[S]$, which relates the incident and the scattered electric fields.

Quad-polarimetric SAR systems measure 2×2 complex scattering matrix $[S]$ associate with each resolution cell in the image. In the case of backscattering in a reciprocal medium, according to the reciprocity theorem, the 3D lexicographic scattering vector $\vec{k}_{\mathrm{L}}$ is obtained as

$$\vec{k}_{\mathrm{L}} = \left[S_{\mathrm{HH}}, \sqrt{2}S_{\mathrm{HV}}, S_{\mathrm{VV}}\right]^{T}. \tag{1}$$

The inherent speckle in the SAR data must be reduced by spatial averaging at the expense of loss of spatial resolution. In this case, a more appropriate representation of the backscattering signal is the covariance matrix. The average covariance matrix $\langle [C] \rangle$ is defined by $\vec{k}_{\mathrm{L}}$, shown as

$$\begin{aligned}\langle [C] \rangle &= \left\langle \vec{k}_{\mathrm{L}} \vec{k}_{\mathrm{L}}^{*T} \right\rangle \\ &= \begin{bmatrix} \langle S_{\mathrm{HH}} S_{\mathrm{HH}}^{*} \rangle & \langle \sqrt{2} S_{\mathrm{HH}} S_{\mathrm{HV}}^{*} \rangle & \langle S_{\mathrm{HH}} S_{\mathrm{VV}}^{*} \rangle \\ \langle \sqrt{2} S_{\mathrm{HV}} S_{\mathrm{HH}}^{*} \rangle & \langle 2 S_{\mathrm{HV}} S_{\mathrm{HV}}^{*} \rangle & \langle \sqrt{2} S_{\mathrm{HV}} S_{\mathrm{VV}}^{*} \rangle \\ \langle S_{\mathrm{VV}} S_{\mathrm{HH}}^{*} \rangle & \langle \sqrt{2} S_{\mathrm{VV}} S_{\mathrm{HV}}^{*} \rangle & \langle S_{\mathrm{VV}} S_{\mathrm{VV}}^{*} \rangle \end{bmatrix},\end{aligned} \tag{2}$$

where $\langle \cdot \rangle$ denotes the ensemble average in the data processing, and the superscript $*$ denotes complex conjugation.

The covariance matrix is directly related to measurable radar parameters and more straightforward to understand physically.

2.2. Description of MCSM. MCSM regards single-bounce, double-bounce, volume, helix, and wire scattering as the elementary scattering mechanisms in the analysis of Pol-SAR images [8]. Therefore, the covariance matrix can be expressed as the combination of these five components

$$[C] = f_s[C_s] + f_d[C_d] + f_v[C_v] + f_h[C_h] + f_w[C_w], \tag{3}$$

where f_s, f_d, f_v, f_h and $f_w$are the coefficients of single-bounce, double-bounce, volume, helix ,and wire scattering to be determined. $[C_s]$, $[C_d]$, $[C_v]$, $[C_h]$, and $[C_w]$ represent the corresponding covariance basis, respectively. The detailed descriptions of these elementary scattering matrixes are shown in [8]. Comparing the covariance matrix elements, we obtain the following six equations:

$$\begin{aligned}
&\text{(a)} \quad \left\langle |S_{\mathrm{HH}}|^2 \right\rangle = f_s |\beta|^2 + f_d |\alpha|^2 + f_v + \frac{1}{4} f_h + f_w |\gamma|^2, \\
&\text{(b)} \quad \left\langle |S_{\mathrm{VV}}|^2 \right\rangle = f_s + f_d + f_v + \frac{1}{4} f_h + f_w, \\
&\text{(c)} \quad \langle S_{\mathrm{HH}} S_{\mathrm{VV}}^{*} \rangle = f_s \beta + f_d \alpha + \frac{1}{3} f_v - \frac{1}{4} f_h + f_w \gamma, \\
&\text{(d)} \quad \left\langle |S_{\mathrm{HV}}|^2 \right\rangle = \frac{1}{3} f_v + \frac{1}{4} f_h + f_w |\rho|^2, \\
&\text{(e)} \quad \langle S_{\mathrm{HH}} S_{\mathrm{HV}}^{*} \rangle = \pm j \frac{1}{4} f_h + f_w \gamma \rho^{*}, \\
&\text{(f)} \quad \langle S_{\mathrm{HV}} S_{\mathrm{VV}}^{*} \rangle = \pm j \frac{1}{4} f_h + f_w \rho,
\end{aligned} \tag{4}$$

where γ and ρ are the ratio of HH and HV backscattering to VV backscattering, namely, $\gamma = S_{\mathrm{HH}}/S_{\mathrm{VV}}$ and $\rho = S_{\mathrm{HV}}/S_{\mathrm{VV}}$.

The wire scattering coefficient f_w and the helix scattering coefficient f_h can be obtained from (4)(e) and (4)(f), they are shown as follows:

$$\begin{aligned}
f_w &= \left| \frac{\langle S_{\mathrm{HH}} S_{\mathrm{HV}}^{*} \rangle - \langle S_{\mathrm{HV}} S_{\mathrm{VV}}^{*} \rangle}{\gamma \rho^{*} - \rho} \right|, \\
f_h &= 2 \left| \mathrm{Im} \left\{ \langle S_{\mathrm{HH}} S_{\mathrm{HV}}^{*} \rangle + \langle S_{\mathrm{HV}} S_{\mathrm{VV}}^{*} \rangle - f_w (\gamma \rho^{*} + \rho) \right\} \right|, \\
&= 2 \left| \mathrm{Im} \left\{ \left(\langle S_{\mathrm{HH}} S_{\mathrm{HV}}^{*} \rangle + \langle S_{\mathrm{HV}} S_{\mathrm{VV}}^{*} \rangle \right) \left(1 - \frac{f_w}{|S_{\mathrm{VV}}|^2} \right) \right\} \right|.
\end{aligned} \tag{5}$$

Then, (4)(d) gives the volume scattering coefficient f_v directly as

$$f_v = 3 \left\{ \left\langle |S_{\mathrm{HV}}|^2 \right\rangle - \frac{1}{4} f_h - f_w |\rho|^2 \right\}. \tag{6}$$

The remaining unknowns can be obtained in the same manner as shown in [2].

Therefore, the scattering powers P_s, P_d, P_v, P_h, and P_w corresponding to single-bounce, double-bounce, volume, helix, and wire scattering contributions, respectively, are estimated as

$$\begin{aligned}
P_s &= f_s \left(1 + |\beta|^2 \right), \\
P_d &= f_d \left(1 + |\alpha|^2 \right), \\
P_v &= \frac{8 f_v}{3}, \\
P_h &= f_h, \\
P_w &= f_w \left(1 + |\gamma|^2 + 2 |\rho|^2 \right), \\
P &= P_s + P_d + P_v + P_h + P_w.
\end{aligned} \tag{7}$$

Compared with three-component scattering model [2], in MCSM the helix and wire scattering mechanism corresponding to copolar and the cross-polar correlations are introduced for a more general target decomposition theorem.

3. Texture Characteristic of SAR Image

Growing crops display a wide range of canopy geometries and shapes of plant components. Some crops (or at least some of their components) show strongly preferred orientations, such as the stalks or ears of cereals.

Texture is one of the most commonly used features used to analyze and interpret images. Texture is a measure of the variation of the intensity of a surface, quantifying properties such as smoothness, coarseness, and regularity. It is often used as a region descriptor in image analysis.

3.1. Theory of GCM. Gray-level co-occurrence matrix (GCM) is a classical second-order statistical tool and it is very useful to characterize the texture features. It is a representation of the spatial relationship of gray levels in an image, and an important characteristic for the automated or semiautomated interpretation of the digital images. GCM can be specified in a matrix of relative frequencies $p(i, j)$, with which two neighboring pixels are separated by distance d and angle θ, one with gray level i and the other with gray level j, shown as

$$\mathrm{GCM}_{L\times L} = \begin{bmatrix} p(0,0) & p(0,1) & \cdots & p(0,L-1) \\ p(1,0) & p(1,1) & \cdots & p(1,L-1) \\ \cdots & \cdots & p(i,j) & \cdots \\ p(L-1,0) & p(L-1,1) & \cdots & p(L-1,L-1) \end{bmatrix}. \tag{8}$$

A 2D co-occurrence matrix is an $L \times L$ matrix, where L is the number of gray levels within an image. GCM is symmetric and calculated within a sliding window due to the spatial dependence frequencies.

The GCMs are the conditional joint probabilities of all pairwise combinations of the gray levels (i, j) restricted by interpixel distance d and orientation θ in the fixed-size spatial window [15, 16]. For the given distance d, we can get four different GCM P_{0°, P_{45°, P_{90°, and P_{135° at four different orientations $\theta = 0^\circ, 45^\circ, 90^\circ, 135^\circ$, respectively. For different orientations, the distances are given by the following expression:

$$\begin{aligned} &\theta = 0^\circ : |x_1 - x_2| = d, \quad |y_1 - y_2| = 0, \\ &\theta = 45^\circ : x_1 - x_2 = \pm d, \quad y_1 - y_2 = \pm d, \\ &\theta = 90^\circ : |x_1 - x_2| = 0, \quad |y_1 - y_2| = d, \\ &\theta = 135^\circ : x_1 - x_2 = \pm d, \quad y_1 - y_2 = \mp d, \end{aligned} \tag{9}$$

where (x_1, y_1) and (x_2, y_2) are the locations of pixels.

3.2. Extraction of Texture Features. The texture feature of SAR image can be derived by using the GCM method. However, it is very difficult to apply it to interpret the images straightly due to the amount of the data in GCM. To generate the texture features based on the co-occurrence probabilities, the statistics are applied to the probabilities. Generally, these statistics identify some structural aspects of the arrangement of probabilities stored within a matrix, which in turn reflects some qualitative characteristics of the local image texture.

Haralick et al. described 14 different texture features based on GCM at a different angle, which are used for quantitative description of texture features [17]. Based on the theoretical analysis and the feature selection procedure based on Sequential Backward Selection (SBS), four statistical parameters *ENY*, *COR*, *CON*, and *SAV* responding to energy, correlation, contrast, and sum average, respectively, are chosen for texture features in the classification. The definitions of these parameters are shown as follows [17, 18].

(1) *ENY* (energy)

$$ENY = \sum_{i=0}^{L-1}\sum_{j=0}^{L-1} p^2(i,j). \tag{10}$$

ENY is a measurement of the uniformity of local gray and the distribution of texture in SAR image. If gray distribution of SAR image is uniform in a local area, namely, wide texture exists, then *ENY* has a big value; the reverse is also true.

(2) *COR* (correlation):

$$COR = \sum_{i=0}^{L-1}\sum_{j=0}^{L-1} \frac{(i-\mu_x)\left(j-\mu_y\right)p(i,j)}{\sigma_x\sigma_y}, \tag{11}$$

where

$$\begin{aligned} &\mu_x = \sum_i i\sum_j p(i,j), \quad \sigma_x = \sum_i (i-\mu_x)^2\sum_j p(i,j), \\ &\mu_y = \sum_j j\sum_i p(i,j), \quad \sigma_y = \sum_j \left(j-\mu_y\right)^2\sum_i p(i,j). \end{aligned} \tag{12}$$

COR is a measurement of the correlation in the local SAR image, and it is the description of the similarity degree of elements in row or line of GCM. Take the horizontal texture, for example, the *COR* at $\theta = 0^\circ$ is markedly bigger than the other three directions.

(3) *CON* (contrast):

$$CON = \sum_{i=0}^{L-1}\sum_{j=0}^{L-1} (i-j)^2 p(i,j). \tag{13}$$

CON is a measurement of the variation of local gray in SAR image. *CON* can be considered as the definition of image, namely, the definition of texture. The deeper textures are, the bigger *CON* is, and the clearer visual effect of the image is. In the image, *CON* of narrow texture is big whereas *CON* of wide texture is small. For a texture, the *CON* along the texture is small whereas *CON* cross the texture is big.

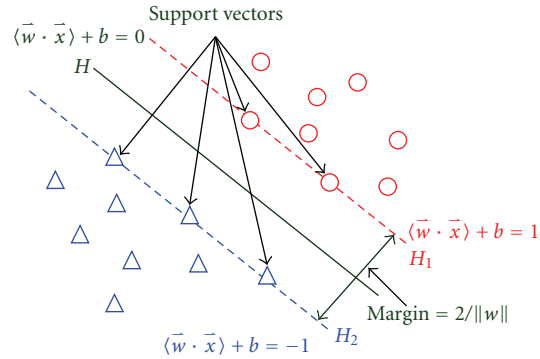

Figure 1: Fundamental idea of OSH and margin.

(4) SAV (sum average):

$$SAV = \sum_{n=0}^{2L-2} \sum_{i=0}^{L-1} \sum_{\substack{j=0 \\ i+j=n}}^{L-1} np(i,j) = \sum_{n=0}^{2L-2} n \sum_{i=0}^{L-1} \sum_{\substack{j=0 \\ i+j=n}}^{L-1} \hat{p}(i,j) = \sum_{n=0}^{2L-2} n\hat{p}_{i+j}(n)\,. \tag{14}$$

SAV is a measurement of the average energy of local gray in SAR image. It is a conditional average under the condition of the sum of x coordinate and y coordinate equals to n.

4. Support Vector Machine (SVM)

SVM is based on statistical learning theorem's VC Dimension concept and Structure Risk Minimization (SRM) principle [12, 13]. Its fundamental idea is that the feature of input space is mapped into a high-dimensional feature space through nonlinear transformation. Then the Optimal Separating Hyperplane (OSH) is established in the feature space. The nonlinear transformation is implemented by defining proper kernel function. SVM has two important features. Firstly, the upper bound on the generalization error does not depend on the dimension of the space. Secondly, the error bound is minimized by maximizing the margin, that is, the minimal distance between the hyperplane and the closest data points.

4.1. Linear Classification and OSH. SVM is developed from OSH of linear separable case. For the training samples, $(\vec{x}_1, y_1), \ldots, (\vec{x}_l, y_l)$, $\vec{x}_i \in R^n$, $y_i \in \{-1, +1\}$, where $\vec{x}$ is an n-dimensional vector, y is the corresponding class labels of $\vec{x}$. l is the number of the training sample.

SVM is a binary classifier, and its decision function can be expressed as $\operatorname{sgn}(f(\vec{x}))$. The object of SVM is looking for a function $f(\vec{x})$, satisfying $y_i \cdot \operatorname{sgn}(f(\vec{x})) > 0$. For linear separable case, the decision function can be described by

$$f\left(\vec{x}\right) = \left\langle \vec{w} \cdot \vec{x} \right\rangle + b \quad \left(\vec{w} \in R^n, b \in R\right), \tag{15}$$

where $\langle \cdot \rangle$ denotes inner product.

The feature space of two types of samples can be separated by hyperplane $\langle \vec{w} \cdot \vec{x} \rangle + b = 0$. Figure 1 depicts an example of geometry in two-dimensional feature space. In Figure 1, H, H_1, and H_2 are the separating hyperplane, triangular point and circle point represent two types of samples. The sample data on H_1 and H_2 are called support vectors, which satisfy $\langle \vec{w} \cdot \vec{x} \rangle + b = 1$ or $\langle \vec{w} \cdot \vec{x} \rangle + b = -1$. The distance between the separating hyperplane is called margin.

SVM is able to use a few support vectors to represent the whole sample set. The so-called optimal classification requires the two types of samples be correctly separated (i.e., training error trends towards 0) and the margin be maximized. Hence the rest data will satisfy the following constraint:

$$y_i \cdot \operatorname{sgn}\left(\left\langle \vec{w} \cdot \vec{x}_i \right\rangle + b\right) \geq 1 \quad (i = 1, \ldots, l). \tag{16}$$

The margin between H_1 and H_2 is $2/\|w\|$. So the problem of looking for OSH under maximal margin condition can be converted to searching for the minimum of $\|w\|/2$, constrained by (16).

Using Lagrangian method, the optimal weight coefficient of OSH $\vec{w}^*$ and the threshold of the classifier b^* can be obtained through any couple of support vectors of the two types. Then the optimal separating decision function can be obtained

$$f\left(\vec{x}\right) = \operatorname{sgn}\left\{\left\langle \vec{w}^* \cdot \vec{x} \right\rangle + b^*\right\} = \operatorname{sgn}\left\{\sum_{x_i \in sv} a_i^* y_i \left\langle \vec{x}_i \cdot \vec{x} \right\rangle + b^*\right\}. \tag{17}$$

4.2. Nonlinear Classification. Mostly, classification of SAR images seems not to be linearly separable because of the speckle. As for nonlinear case, two kinds of extension of SVM are proposed [12, 13]. One is a soft margin of Lagrangian multipliers a_i. A slack variable C is introduced in the constraint $a_i \geq 0$, that is, $0 \leq a_i \leq C$, to remove the effect of the outliers. Here C is a specified constant and controls the punishing degree to incorrectly separated samples. This strategy achieves a compromise between maximizing the distance between hyperplane and nearest training samples and minimizing the separating error.

The other and the most common is the kernel function based on nonlinear mapping. To get a potentially better representation of the data, we can map the data points into an alternative space, generally called feature space, through a replacement. The so-called kernel function $K(x_i, x)$ is chosen to replace the inner product in (17), and then the corresponding decision function is

$$f(x) = \operatorname{sgn}\left\{\sum_{x_i \in sv} a_i^* y_i K\left(\vec{x}_i \cdot \vec{x}\right) + b^*\right\}. \tag{18}$$

The replacement of inner product $\langle x_i, \vec{x} \rangle$ by $K(x_i, \vec{x})$ in the OSH is equivalent to changing a nonlinear problem in

original space into a linear one in high-dimensional space, and looking for the OSH in the converted space. In the kernel method, explicit representation or computation of the mapping is never needed. One of the most popular kernels is the Gaussian kernel, defined by

$$K\left(\vec{x}_i, \vec{x}_j\right) = \exp\left(-\frac{\left\|\vec{x}_i - \vec{x}_j\right\|^2}{2\sigma^2}\right). \tag{19}$$

With a suitable choice of kernel the data can become separable in feature space despite being nonseparable in the original input space.

4.3. Multiclassifier. For classifications, the samples should be divided into generally more than two kinds. Since SVM is a binary classifier, multi-classifier should be formed for multiclassification problem. There are always two ways for multi-classifier.

One is one-against-rest method. The sample data of the i type are used as positive training samples for the classifier, and the samples of the rest types used as negative ones. At last the bigger data of the output from the binary classifier is exported. For N type problem, it needs N binary classifiers.

The other is one-against-one method, and it needs $k = N(N-1)/2$ binary classifiers. This method constructs all the binary classifier between all the types, and votes for the type of the samples.

5. Classification of PolSAR Image Based on MCSM and SVM

5.1. Experiment Data. The SAR data used in the study were acquired by the fully polarimetric Danish airborne SAR system, ElectroMagnetic Institute Synthetic Aperture Radar (EMISAR) which operates at two frequencies, C-band (5.3 GHz/5.7 cm wavelength) and L-band (1.25 GHz/24 cm wavelength). The nominal one-look spatial resolution is 2×2 m (one-look); the ground range swath is approximately 12 km and typical incidence angles range from 35° to 60°. The processed data from this system are fully calibrated using an advanced internal calibration system [19, 20]. In 1998 simultaneous L- and C-band data were acquired over the Foulum agricultural test site in Jutland, Denmark, on 21 March, 17 April, 20 May, 16 June, 15 July, and 16 August.

The test data are the complex covariance format of L-band fully polarimetric images of Foulum Area (DK), acquired on April 17, 1998. The six different product images are spatially averaged and resampled at a 5 m × 5 m ground pixel spacing using a low-pass filter.

The crop types present in the area are the spring crops (beets, peas, potatoes, spring barley, and spring rape) and the winter crops (grass, winter barley, winter wheat, and winter rape), where spring and winter barley, winter wheat, and winter rape are the dominant crop types [19]. Due to lack of the corresponding groundtruth, just five broad classes are fixed to classified the image, that is, building, forest, bare field, broad leaves crops, and small stem crops [20].

The optical image and HH channel image are shown in Figures 2(a) and 2(b), respectively.

5.2. The Procedure of Classification. The procedure of classification based on MCSM and SVM consists of the following.

(1) Obtain the features of PolSAR data. Decompose the PolSAR data using MCSM to obtain the scattering powers of five scattering mechanisms. Calculate the texture features of SAR images based on gray co-occurrence matrix.

(2) Select features used in the classification and settle the form of feature vectors. Based on the theoretical and experimental analyses, it is found that with the decreasing number of support vector, the precision of classification increases. Then the number of support vector is considered as a measurement of feature extraction. The Sequential Backward Selection (SBS) is chosen in the selection procedure, in which the features are sequentially removed from a full candidate set until the removal of further features increases the criterion.

(3) Normalize the features. Because the meanings of different features are different, the ranges of these features are rather different generally.

(4) Extract training samples from the representative area of each class in the SAR image.

(5) Train the classifier using training samples; determine the decision function, kernel function, and parameters of SVM in the learning procedure of training data.

(6) Select the testing samples of each class, and calculate the precision of classification result.

(7) Classify the total SAR image using the trained classifier.

5.3. Polarimetric Decomposition with MCSM. As is known, in forest area the predominate scattering mechanism is volume scattering which shows that the high backscattering comes from direct backscattering from the prosperous leaves. The backscattering is dominated by surface scattering from the bare fields. Broad leaves crops primarily present volume scattering; whereas the small stem crops mostly present double-bounce surface-vegetation scattering due to the penetration of L band electromagnetic wave. In urban area building blocks produce a rather predominant HV response, therefore, the helix and wire scattering component appears stronger in these areas.

Figure 3 shows the decomposition result of MCSM, Figures 3(a)–3(e) are the scattering power image of each scattering mechanism, respectively. From the results of MCSM, we found that double-bounce, helix, and wire scattering are prominent for the buildings, especially at the edge of buildings. The scattering power of buildings in the upper right and lower right become stronger compared with HH channel image in Figure 2(b). The forest area on the left

(a) (b)

Figure 2: EMISAR test data of Foulum Area (DK): (a) optical image, (b) HH channel image.

presents a rather strong scattering power indicating volume scattering is prominent.

Figure 3(f) is the pseudo-colour image of the MCSM decomposition, which is coloured by P_d (red), P_v (green), and P_s (blue). The forest area and the residential areas represent strong scattering. Most of the small stem crop farmlands are purple, where double-bounce and surface scattering are equally strong due to the penetration of electromagnetic wave. Some broad leaves crop farmlands only present volume scattering, and they are green in the Figure 3. The blue areas in left and upper right correspond to the bare field, which shows that the surface scattering is predominant in these areas.

5.4. Classification Result Based on Cameron Decomposition. Cameron decomposition is a classical unsupervised method in PolSAR image classification, in which the polarization scattering matrix can be decomposed into several typical scattering types based on the scattering mechanism [21]. The basis of Cameron decomposition is the reciprocity and symmetry of target.

Using Cameron decomposition, the test EMISAR data is classified into six typical classes, that is, trihedral, diplane, dipole, cylinder, narrow diplane, and 1/4 wave device. Figure 4 is the classification result of EMISAR image based on Cameron decomposition. Comparing the scattering mechanisms in Figure 4 and the ground types in Figure 5, we can find out the corresponding relationship. The trihedral scattering corresponding to the single-bounce scattering represents the bare field. The diplane scattering corresponding to surface-vegetation dihedral structures and stems in the small stem crops. The random dipole scattering produces the volume scattering, which is the primary scattering in forest. The narrow diplane is a typical scattering in urban area due to the dihedral structures of building and ground. Conclusively, the Cameron decomposition can almost express the elementary scattering mechanism. However, Cameron decomposition does not take the surrounding information into account, and it will not obtain a very good classification result.

5.5. Classification Result Based on MCSM and SVM. In the supervised classification procedure, 120 pixels are selected for each type as training samples. The scattering powers of MCSM and the texture features are chosen to obtain the feature set as (P_s, P_d, P_v, P_h, P_w, ENY_{HH}, COR_{HH}, CON_{HH}, SAV_{HH}, ENY_{HV}, COR_{HV}, CON_{HV}, SAV_{HV}, ENY_{VV}, COR_{VV}, CON_{VV}, SAV_{VV}). In the feature set, P_s, P_d, P_v, P_h, and P_w are the scattering powers of single-bounce, double-bounce, volume, helix, and wire scattering components, respectively. The texture features ENY, COR, CON, and SAV obtained from GCM are energy, correlation, contrast, and sum average, respectively. The subscripts of HH, HV, and VV represent the polarimetric channel of SAR image, respectively. Combining these features, not only the polarimetric information of objects but also the texture features of SAR image are used in the classification procedure. Namely based on the difference of polarimetric information of a pixel and its surroundings, the pixels are classified into different classes.

The SVM classifier is designed by selecting Gaussian RBF kernel as a kernel function. In this paper, the one-against-one method is used to construct the multi-classifier to solve the multi-classification problem. Use the feature set of training samples as the input of SVM, and acquire the parameters $\vec{w}^*$ and b^* of the SVM classifier.

In order to give a quantitative analysis of the proposed classification method, we select 1330 test samples of the five classes, respectively, to test the classification method. Table 1 is the classification result of these test samples. The precisions of building, forest, bare field, small stem crops and broad leaves crops are 84.0%, 72.6%, 94.4%, 79.5%, and 92.9%, respectively. And the total precision of the test data is 84.7%. Some pixels of forest are wrongly classified as building

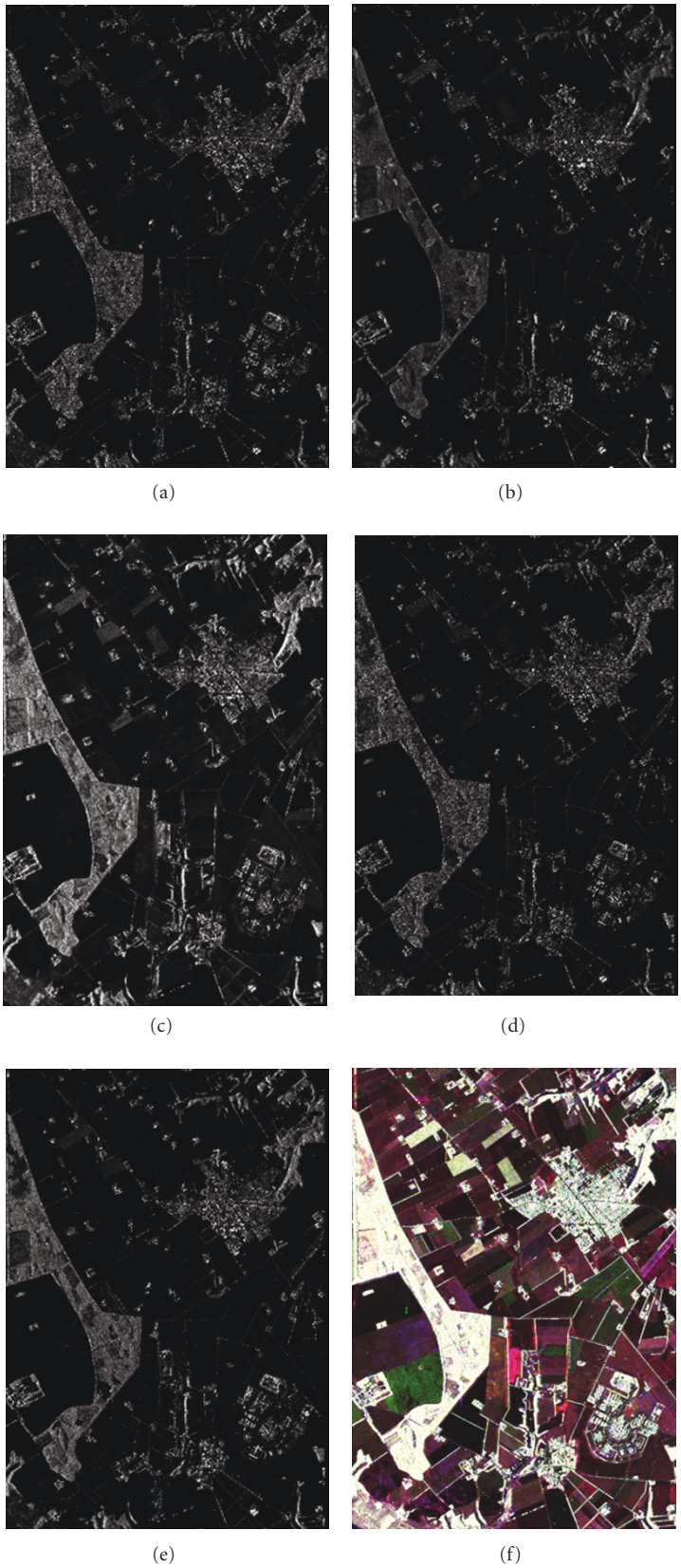

(a) (b) (c) (d) (e) (f)

Figure 3: Polarimetric decomposition image of MCSM: (a) power image of P_s, (b) power image of P_d, (c) power image of P_v, (d) power image of P_h, (e) power image of P_w, (f) pseudo-colour decomposition result; the image is colored by P_d (red), P_v (green), and P_s (blue).

Table 1: The classification result of test pixels.

	Class					
Test	Building	Forest	Bare field	Small stem crop	Broad leaves crop	Precision
Building	1117	213	0	0	0	84.0%
Forest	364	965	0	0	1	72.6%
Bare field	0	0	1255	75	0	94.4%
Small stem crop	0	0	22	1057	251	79.5%
Broad leaves crop	8	13	0	74	1235	92.9%

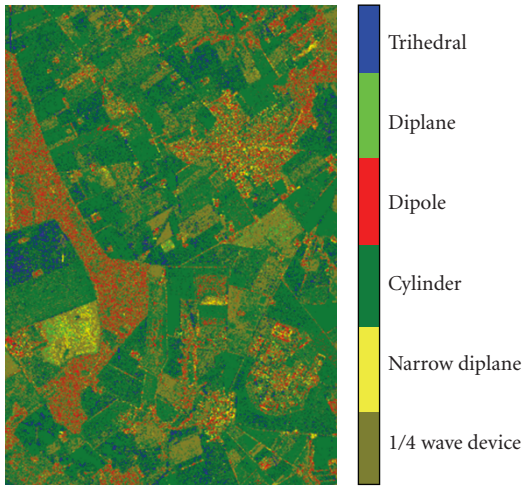

Figure 4: Classification of EMISAR image based on Cameron decomposition.

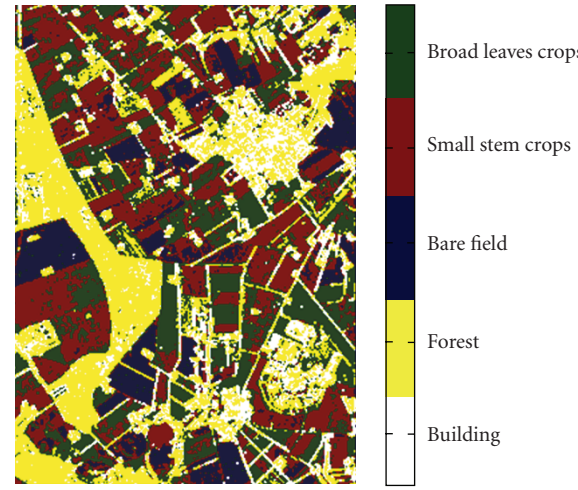

Figure 5: Classification of EMISAR image based on MCSM and SVM.

because they both present double-bounce scattering. A few small stem crops are wrongly classified as broad leaves crop mainly because of their prosper foliage. Conclusively, the classification using MCSM and GCM features can obtain a relative accurate result.

Then the classifier can be used to classify the image. Finally, the test image is classified with the trained SVM classifier. The classification result of test data based on MCSM and SVM is shown in Figure 5.

Comparing Figure 5 with the optical image in Figure 2(a) and the classification result in [20], we can find the PolSAR image has been well classified. It is clear that the classification for the individual fields is coherent; that is, most of the pixels belonging to a specific field are classified as the same category. The forest, buildings, bare field can be discriminated from each other very well. The forest areas are distinctly distinguished with other types due to particular strong scattering power. The buildings are almost correctly classified and a few are wrongly fixed into forest owing to the surrounding trees around the houses. The bare field can be well classified from other types mainly due to the texture feature of plowing direction. The farmland can be distinguished with other types; however some small stem crops and broad leaves crops are in some sort mixed classified, because the two classed of targets have some similar features. The broad leaves crops show mainly volume scattering; whereas the small stem crops present both the double-bounce and volume scattering.

6. Discussion and Conclusion

MCSM is a general polarimetric target decomposition method, which can be applied to the symmetry and asymmetry reflection conditions. SVM is a popular algorithm based on statistical learning theorem's VC dimension concept and structural risk minimization principle, and it is considered as a good candidate because of its high generalization performance. Texture is one of the most commonly used features used to analyze and interpret images. By combining MCSM, texture of GCM and SVM, we propose a new PolSAR image classification algorithm. The quantitative analysis and the classification results with the implementation of EMISAR L band fully polarimetric data show that the proposed approach is accurate and effective for polarimetric classification. The comparisons with typical classification methods will be further discussed.

Acknowledgments

The authors would like to acknowledge Professor Henning SKIVER and Dr. Jorgen DALL for providing the test data.

This work received support from the National Natural Science Foundation of China, no. 6067209 and no. 60872098.

References

[1] S. R. Cloude and E. Pottier, "An entropy based classification scheme for land applications of polarimetric SAR," *IEEE Transactions on Geoscience and Remote Sensing*, vol. 35, no. 1, pp. 68–78, 1997.

[2] A. Freeman and S. L. Durden, "A three-component scattering model for polarimetric SAR data," *IEEE Transactions on Geoscience and Remote Sensing*, vol. 36, no. 3, pp. 963–973, 1998.

[3] L. Ferro-Famil, E. Pottier, and J.-S. Lee, "Unsupervised classification of multifrequency and fully polarimetric SAR images based on the H/A/Alpha-Wishart classifier," *IEEE Transactions on Geoscience and Remote Sensing*, vol. 39, no. 11, pp. 2332–2342, 2001.

[4] J.-S. Lee, M. R. Grunes, E. Pottier, and L. Ferro-Famil, "Unsupervised terrain classification preserving polarimetric scattering characteristics," *IEEE Transactions on Geoscience and Remote Sensing*, vol. 42, no. 4, pp. 722–731, 2004.

[5] S. R. Cloude and E. Pettier, "A review of target decomposition theorems in radar polarimetry," *IEEE Transactions on Geoscience and Remote Sensing*, vol. 34, no. 2, pp. 498–518, 1996.

[6] T. Moriyama, S. Uratsuka, T. Umehara, et al., "Polarimetric SAR image analysis using model fit for urban structures," *IEICE Transactions on Communications*, vol. E88-B, no. 3, pp. 1234–1242, 2005.

[7] Y. Yamaguchi, T. Moriyama, M. Ishido, and H. Yamada, "Four-component scattering model for polarimetric SAR image decomposition," *IEEE Transactions on Geoscience and Remote Sensing*, vol. 43, no. 8, pp. 1699–1706, 2005.

[8] L. Zhang, B. Zou, H. Cai, and Y. Zhang, "Multiple-component scattering model for polarimetric SAR image decomposition," *IEEE Geoscience and Remote Sensing Letters*, vol. 5, no. 4, pp. 603–607, 2008.

[9] M. Hellmann, G. Jaeger, E. Kraetzschmar, and M. Habermeyer, "Classification of full polarimetric SAR-data using artificial neural networks and fuzzy algorithms," in *Proceedings of the International Geoscience and Remote Sensing Symposium (IGARSS '99)*, vol. 4, pp. 1995–1997, Hamburg, Germany, June-July 1999.

[10] S. Fukuda and H. Hirosawa, "Polarimetric SAR image classification using support vector machines," *IEICE Transactions on Electronics*, vol. E84-C, no. 12, pp. 1939–1945, 2001.

[11] S. Fukuda, R. Katagiri, and H. Hirosawa, "Unsupervised approach for polarimetric SAR image classification using support vector machines," in *Proceedings of the International Geoscience and Remote Sensing Symposium (IGARSS '02)*, vol. 5, pp. 2599–2601, 2002.

[12] V. N. Vapnik, *Statistical Learning Theory*, John Wiley & Sons, New York, NY, USA, 1998.

[13] V. N. Vapnik, "An overview of statistical learning theory," *IEEE Transactions on Neural Networks*, vol. 10, no. 5, pp. 988–999, 1999.

[14] Y. Wang, J. Lu, and X. Wu, "New algorithm of target classification in polarimetric SAR," *Journal of Systems Engineering and Electronics*, vol. 19, no. 2, pp. 273–279, 2008.

[15] F. Argenti, L. Alparone, and G. Benelli, "Fast algorithms for texture analysis using co-occurrence matrices," *IEE Proceedings F: Radar and Signal Processing*, vol. 137, no. 6, pp. 443–448, 1990.

[16] R. W. Conners and C. A. Harlow, "Toward a structural textural analyzer based on statistical methods," *Computer Graphics and Image Processing*, vol. 12, no. 3, pp. 224–256, 1980.

[17] R. M. Haralick, K. Shanmugam, and I. Dinstein, "Textural features for image classification," *IEEE Transactions on Systems, Man and Cybernetics*, vol. 3, no. 6, pp. 610–621, 1973.

[18] A. Baraldi and F. Parmiggiani, "An investigation of the textural characteristics associated with gray level cooccurrence matrix statistical parameters," *IEEE Transactions on Geoscience and Remote Sensing*, vol. 33, no. 2, pp. 293–304, 1995.

[19] H. Skriver, M. T. Svendsen, and A. G. Thomsen, "Multitemporal C- and L-band polarimetric signatures of crops," *IEEE Transactions on Geoscience and Remote Sensing*, vol. 37, no. 5, pp. 2413–2429, 1999.

[20] H. Skriver, J. Dall, T. Le Toan, et al., "Agriculture classification using POLSAR data," in *Proceedings of the 2nd International Workshop on Applications of SAR Polarimetry and Polarimetric Interferometry (POLinSAR '05)*, January 2005.

[21] W. L. Cameron, N. N. Youssef, and L. K. Leung, "Feature motivated polarization scattering matrix decomposition," in *Proceedings of the IEEE International Radar Conference*, pp. 549–557, Arlington, Va, USA, May 1990.